Supporting Information

Efficient Carrier Transfer Induced by Au Nanoparticles for Photoelectrochemical Nitrogen Reduction

Jiaxin Liu,[a,b] Fengying Zhang,[a,b] Haoran Wu,[b] Yuman Jiang,[b] Peng Yang,[b] Wei Zhang,[d] Heng Guo,*[a,b] Yuehan Cao,[b] Guidong Yang[c] and Ying Zhou*[a,b]*

[a] State Key Laboratory of Oil and Gas Reservoir Geology and Exploitation, Southwest Petroleum University, Chengdu 610500, China.

[b] School of New Energy and Materials, Southwest Petroleum University, Chengdu 610500, China.

[c] XJTU-Oxford Joint International Research Laboratory of Catalysis, School of Chemical Engineering and Technology, Xi'an Jiaotong University, Xi'an 7010049, China.

[d] School of Physics and Materials Science, Guangzhou University, Guangzhou 510006, China.

1. Experimental Section

1.1 Materials

Titanium dioxide (TiO_2, 99.8% metals basis), Ethyl cellulose ($(C_{12}H_{22}O_5)_n$, CP), Salicylic acid ($C_7H_6O_3$, AR), Sodium citrate tribasic dihydrate ($C_6H_5Na_3O_7 \cdot H_2O$, AR), para-(dimethylamine)benzaldehyde ($C_9H_{11}NO$, AR) and Sodium hypochlorite solution (NaClO, AR) were purchased from Aladdin Reagent Corp. Sodium nitroprusside ($C_5H_4FeN_6Na_2O_3$, AR) were purchased from Sigma-Aldrich. Chloroauric acid ($HAuCl_4$, 48~50% Au basis) and Triton X-100 ($C_{14}H_{22}O(C_2H_4O)_n$, AR) were purchased from Macklin Reagent Corp. Sodium Carbonate Anhydrous (Na_2CO_3, AR), Sodium borohydride ($NaBH_4$, AR), Sulfuric Acid (H_2SO_4), Hydrochloric Acid (HCl, 36~38%), sodium hydroxide (NaOH, GR) and Ethanol (C_2H_6O, GR) were purchased from Chengdu Kelong Chemical Reagent Corp. N_2 (99.999%) and Ar (99.999%) were provided by Chengdu Keyuan Gas Corp.

1.2 Characterization

The X-ray diffraction (XRD) data were acquired by a PANalytical X'pert diffractometer (Holland) with a Cu Kα ray (45 kV, 35 mA). The morphologies and compositions of these samples were observed with transmission electron microscopy (TEM) images. High-resolution TEM (HRTEM) images were obtained on a JEOL JEM-F200 (Japan) equipped with an energy dispersive X-ray spectrometer (JED-2300T), operating at 200 kV. The UV-vis diffuse reflectance spectra were recorded at room temperature on a Shimadzu UV-2600 spectrophotometer with an integrating sphere using Ba_2SO_4 as the reflectance standard. And the reflectance is converted into absorption value using the Kubelka-Munk function:

$$F(R_\infty) = K/S = \frac{(1 - R_\infty)^2}{2R_\infty}$$

where K is the absorption coefficient, S is the scattering coefficient, and R_∞ is the limit value of the reflection coefficient R of the infinitely thick samples.

The photoluminescence (PL) spectra measurements were performed using a Hitachi

F-7000 fluorescence spectrophotometer. X-ray photoelectron spectroscopy (XPS, Thermo Scientific K-Alpha) were collected using monochromatic Al Kα X-ray (1486.6 eV) as the excitation source, and the spectra were corrected by C 1s spectra (284.8 eV). Transient absorption spectroscopy was measured by a HARPIA-TA spectroscopy system (HARPIA, Light conversion) using PHAROS (1030 nm, pulse width ~ 190 fs, repetition rate 100 kHz, Light Conversion) as the fundamental laser source.

1.3 Product Analysis

Determination of Ammonia: Indophenol blue method was implemented to determine the concentration of obtained ammonia. Typically, 2 mL of the reaction solution was collected from the cathode chamber into a separate container, and 2 mL of NaOH solution (1 M) containing $C_7H_6O_3$ (5%) and $C_6H_5Na_3O_7 \cdot H_2O$ (5%) was added. Subsequently, 1 mL of NaClO (0.05 M) and 0.2 mL of $C_5FeN_6Na_2O$ (1 wt %) were added to above solution. The absorbance of the solution at 655 nm was measured by UV-vis absorption spectroscopy after keeping for 2 h at ambient environment. The calibration curve was constructed using standard ammonia solution with a serious of concentrations.

Determination of Hydrazine: Watt and Chrisp method was conducted to determine the concentration of obtained N_2H_4. Generally, 2 mL of coloring reagent (a mixture of para-(dimethylamine)benzaldehyde (0.599 g), 3 mL HCl (12 mol L^{-1}) and 30 mL ethanol) was added into 2 mL electrolyte. The absorbance of the solution at 455 nm was measured by UV-vis absorption spectroscopy. The calibration curve was constructed using standard hydrazine hydrate solution with a serious of concentrations.

Calculation of NH_3 Yield Rate: The yield rate of ammonia can be calculated by the following equation:

$$c_{NH_3} = [NH_3] \times V/(t \times A_{cat.})$$

where $[NH_3]$ denotes the concentration of ammonia, V is the volume of electrolyte, t is the duration of electrolysis, and A is the area of catalyst loaded

on the working electrode.

Calculation of Faradaic Efficiency: The Faradaic efficiency can be calculated by the following equation:

$$FE = 3 \times F \times [NH_3] \times V/(17 \times Q)$$

where F is Faraday constant and Q is the total charge passing through the electrode during electrolysis.

1.4 DFT Calculation

All computations were performed in the Vienna ab initio simulation package (VASP) within the framework of the density functional theory (DFT) and the projector augmented plane-wave approach. The plane wave energy cut-off is fixed at 380 eV. In the iterative solution of the Kohn-Sham equation, the energy constraint is established at 10^{-5} eV. The calculation was completed on the 4×4×1 supercell on the (101) surface of anatase TiO_2. A vacuum space exceeding 15 Å was employed to avoid the interaction between two periodic units. For all NRR, the Gibbs free energy (ΔG) was described as follows.

$$\Delta G = \Delta E + \Delta E_{ZPE} - T\Delta S$$

where, ΔE denoted the energy of adsorption, ΔE_{ZPE} represent the zero-point energy changes, T=298.15 K (room temperature), and ΔS is the variations in entropy.

2 Additional tables and figures

Table S1 Annealing conditions for synthesis of catalysts.

Samples	Temperature (℃)	Time (h)
$Au_{3.0}$-TiO_2	80	20
$Au_{4.4}$-TiO_2	400	1
$Au_{6.0}$-TiO_2	400	2

Table S2 Fitting parameters for Au-TiO_2:

$$Y(x) = A * \exp\left(-\left(\frac{1}{\tau_1}\right) * x\right) + B * \exp\left(-\left(\frac{1}{\tau_2}\right) * x\right) + C * \exp\left(-\left(\frac{1}{\tau_3}\right) * x\right)$$

Samples	A	τ_1(ps)	B	τ_2(ps)	C	τ_3(ps)
$Au_{3.0}$-TiO_2	0.61	2.67	0.28	21.30	0.11	400.75
$Au_{4.4}$-TiO_2	0.73	3.55	0.18	19.68	0.09	195.27
$Au_{6.0}$-TiO_2	0.74	3.79	0.17	35.71	0.09	333.94

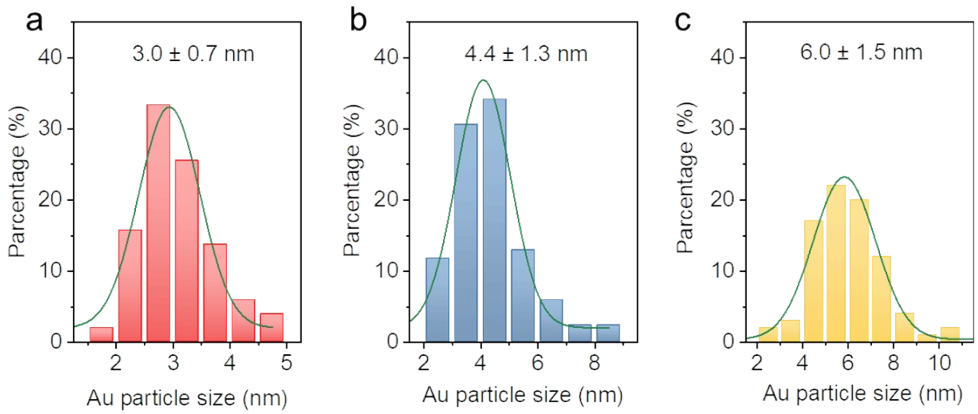

Fig. S1 The size distributions of Au NPs: (a) $Au_{3.0}$-TiO_2, (b) $Au_{4.4}$-TiO_2, and (c) $Au_{6.0}$-TiO_2.

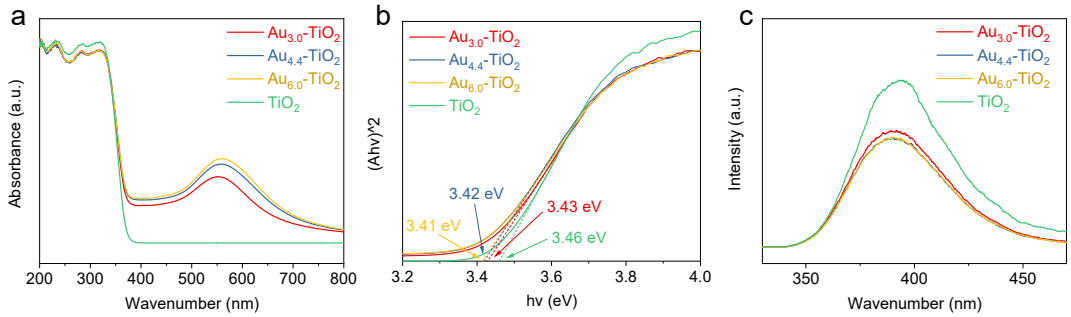

Fig. S2 (a) UV–vis diffuse reflectance spectra; (b) Tauc plots and (c) PL spectra of the samples.

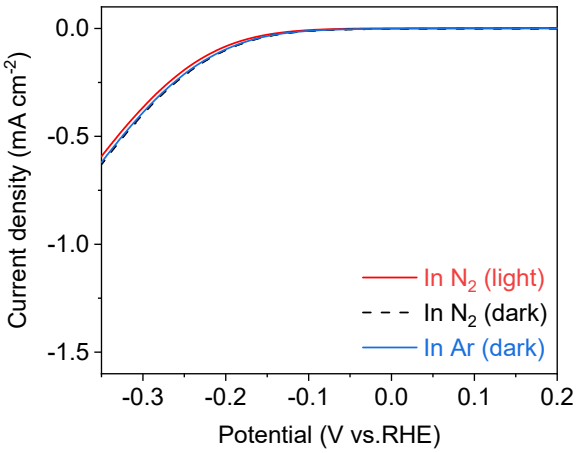

Fig. S3 LSV curves of TiO_2 under different conditions.

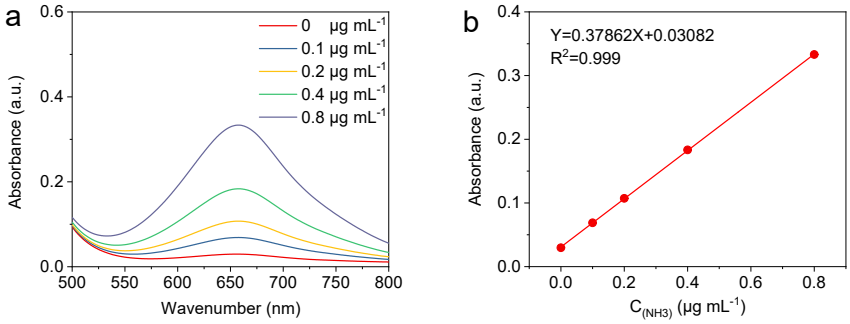

Fig. S4 Calibration curve in 0.05 M H_2SO_4 using ammonium chloride solutions of known concentrations as the standards: (a) UV-vis curves of indophenol assays after incubation for 2 hours; (b) Calibration curve used to determine the NH_3 concentration.

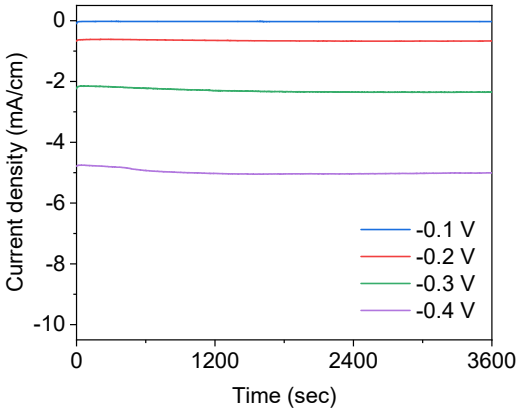

Fig. S5 Chronoamperometric results of Au-TiO_2 at different potentials under illumination.

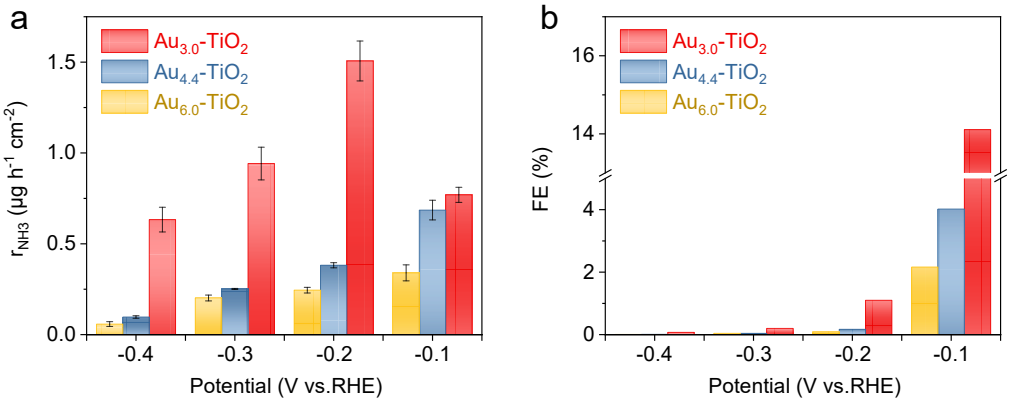

Fig. S6 (a) Ammonia yield rate and (b) Faradaic efficiency of Au-TiO_2.

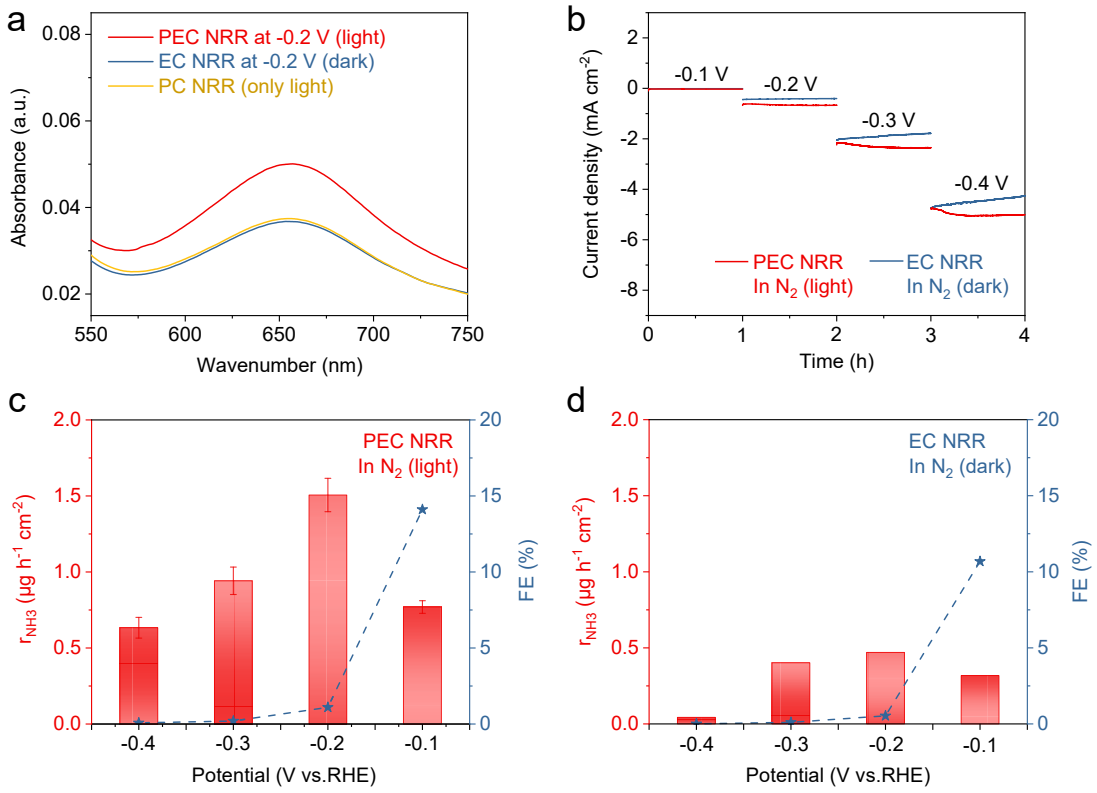

Fig. S7 (a) Absorption spectra of NH_4^+ ions detected by the indophenol blue chromogenic reaction; (b) EC NRR and PEC NRR current-time curves of the $Au_{3.0}$-TiO_2 electrode for various potentials; (c) PEC-NRR ammonia yield rate and Faradaic efficiency; (d) EC-NRR ammonia yield rate and Faradaic efficiency.

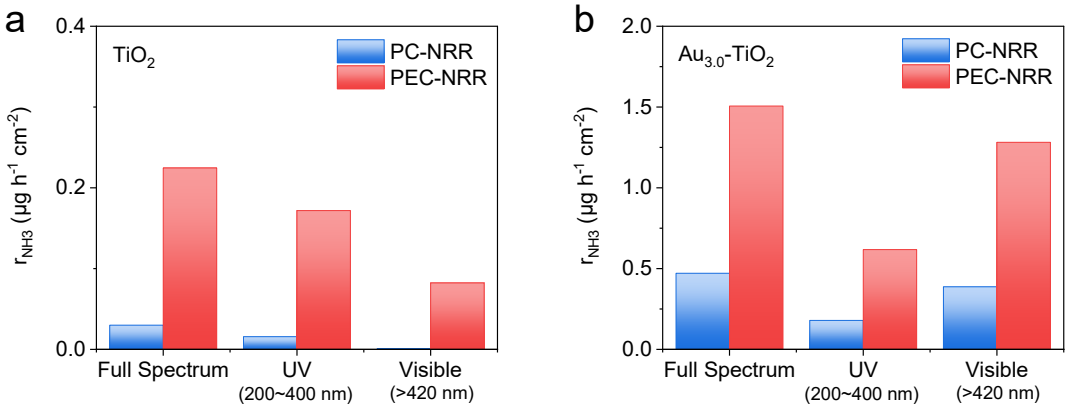

Fig. S8 NH_3 yields for PC-NRR and PEC-NRR of (a)TiO_2 and (b)$Au_{3.0}$-TiO_2 under different wavelength light illumination.

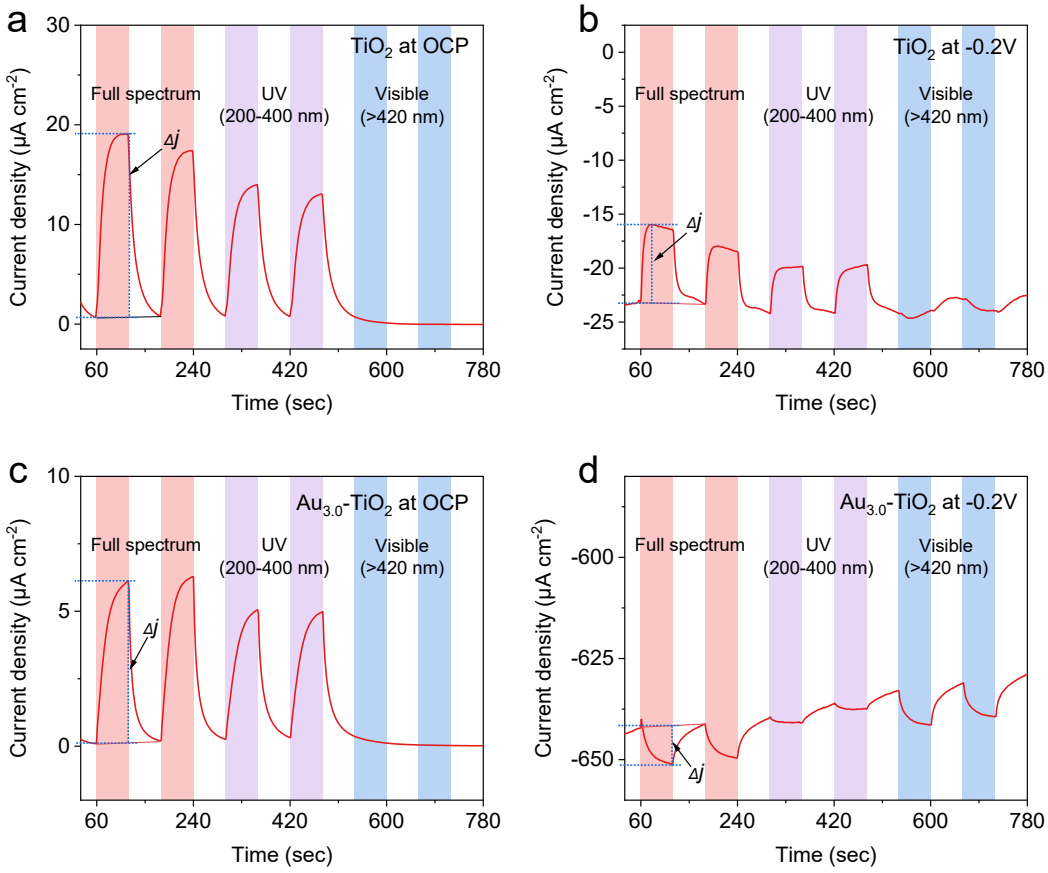

Fig. S9 Photocurrent of (a) TiO_2 at OCP; (b) TiO_2 at -0.2 V; (c) $Au_{3.0}$-TiO_2 at OCP and (d) $Au_{3.0}$-TiO_2 at -0.2 V under different wavelength light illumination.

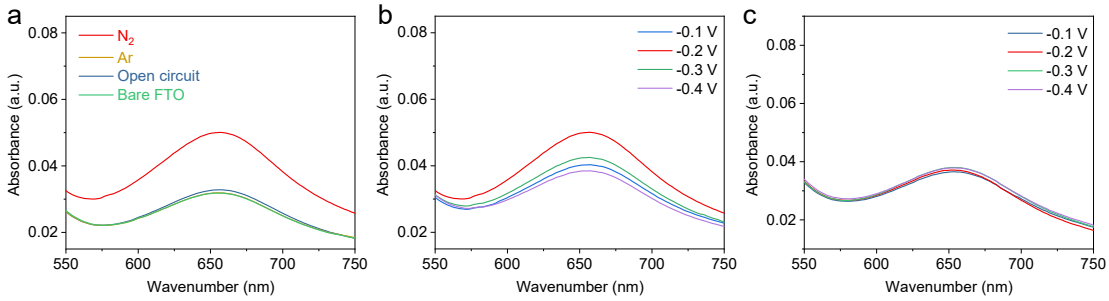

Fig. S10 Absorption spectra of NH_4^+ ions detected by the indophenol blue chromogenic reaction: (a) Control experiment; (b) $Au_{3.0}$-TiO_2 and (c) TiO_2.

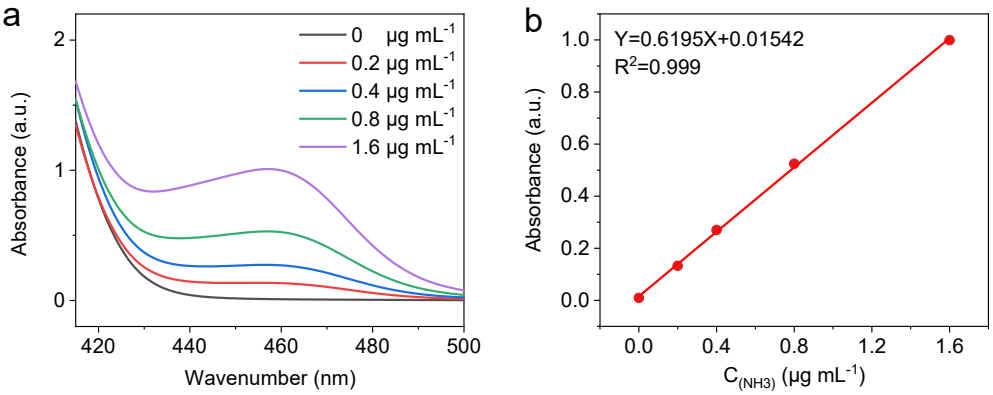

Fig. S11 Calibration curve in 0.05 M H_2SO_4 using hydrazine solutions of known concentrations as the standards: (a) UV-vis curves of various concentrations of hydrazine stained with p-$C_9H_{11}NO$ indicator; (b) Calibration curve used to determine the hydrazine concentration.

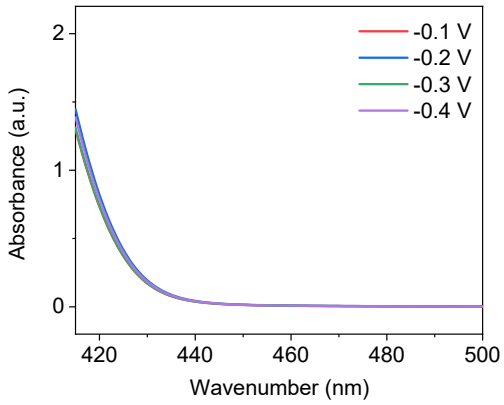

Fig. S12 The absorption spectra of PEC NRR electrolyte for detecting hydrazine.

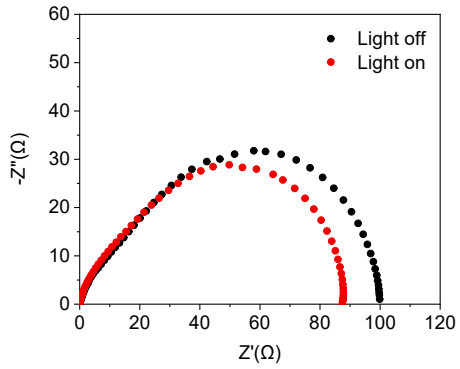

Fig. S13 Electrochemical impedance Nyquist plots of the $Au_{3.0}$-TiO_2 sample at

applied potential of -0.1 V vs. RHE in N_2-saturated 0.05M H_2SO_4 electrolyte.

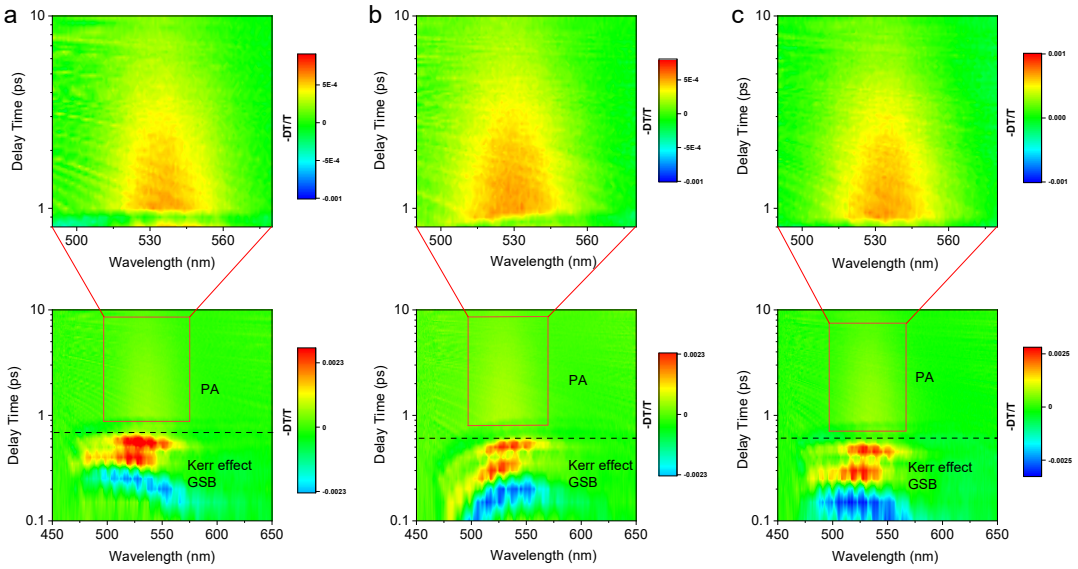

Fig. S14 3D contour plots of TAS observation: (a) $Au_{3.0}$-TiO_2; (b) $Au_{4.4}$-TiO_2 and (c) $Au_{6.0}$-TiO_2.

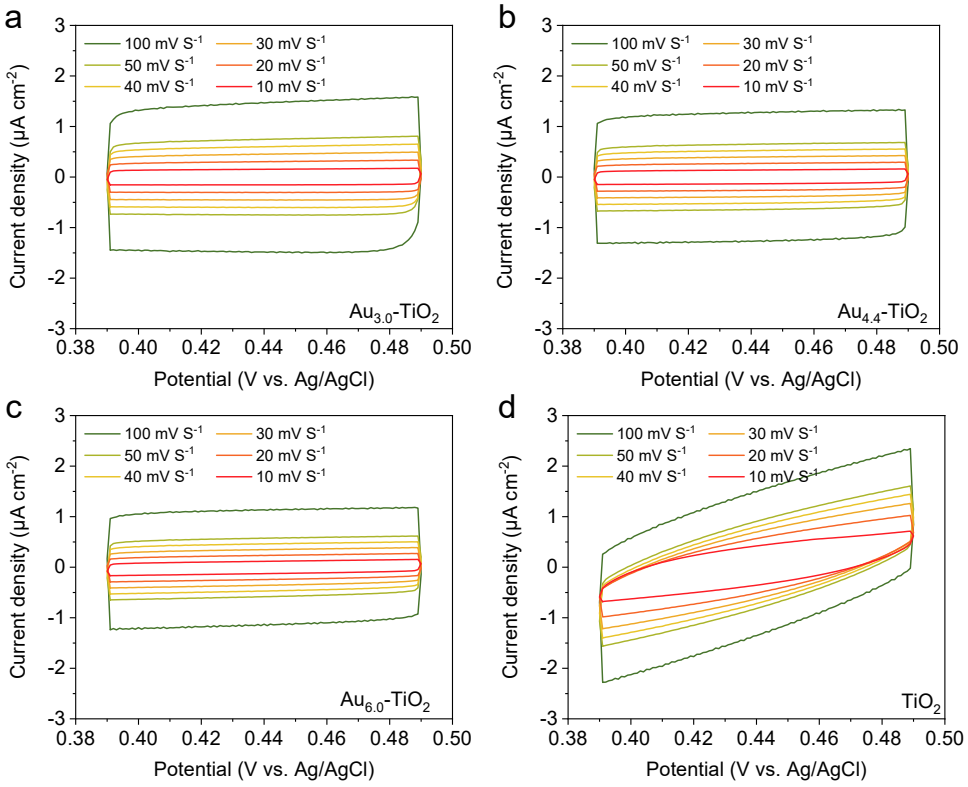

Fig. S15 CV conducted at potentials from -0.49 to 0.39 V vs Ag/AgCl at scanning rates of 10, 20, 30, 40, 50 and 100 $mV \cdot s^{-1}$ for (a) $Au_{3.0}$-TiO_2, (b) $Au_{4.4}$-TiO_2, (c) $Au_{6.0}$-TiO_2 and (d) TiO_2.

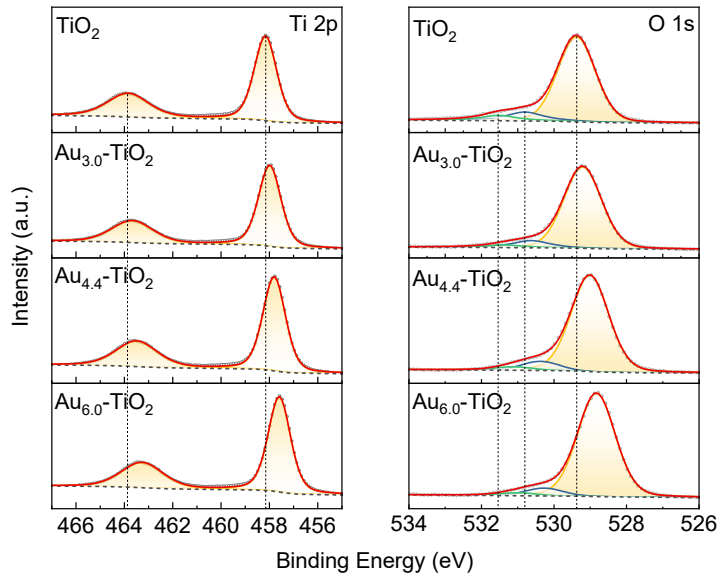

Fig. S16 High-resolution XPS spectra in the Ti 2p and O 1s regions.

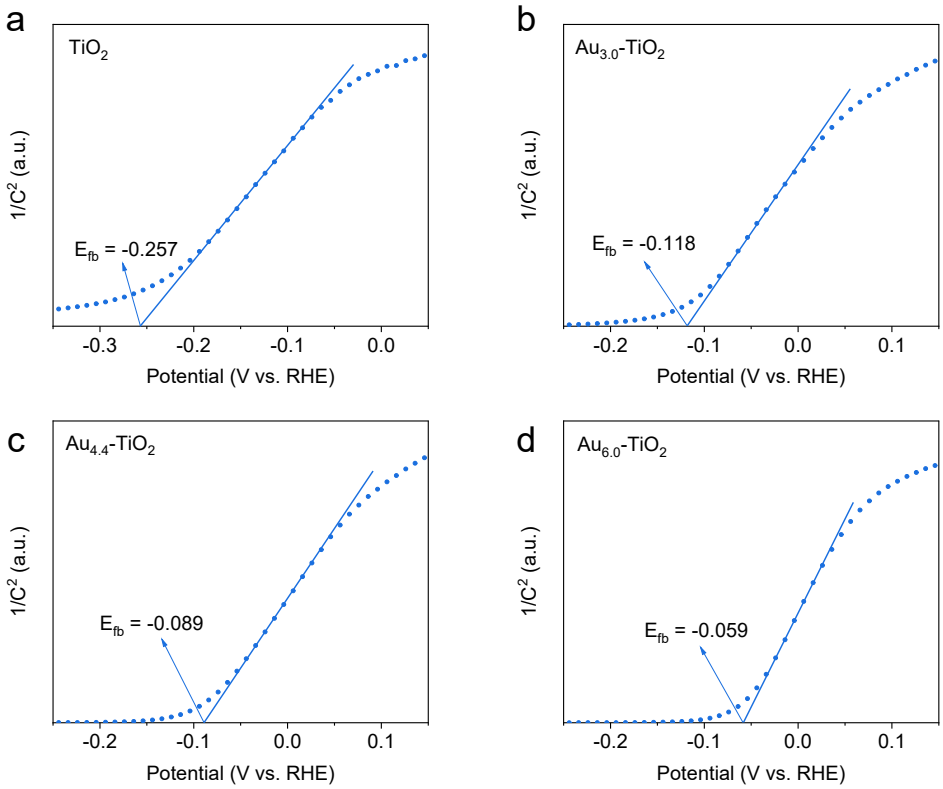

Fig. S17 Mott-Schottky plot of the samples.

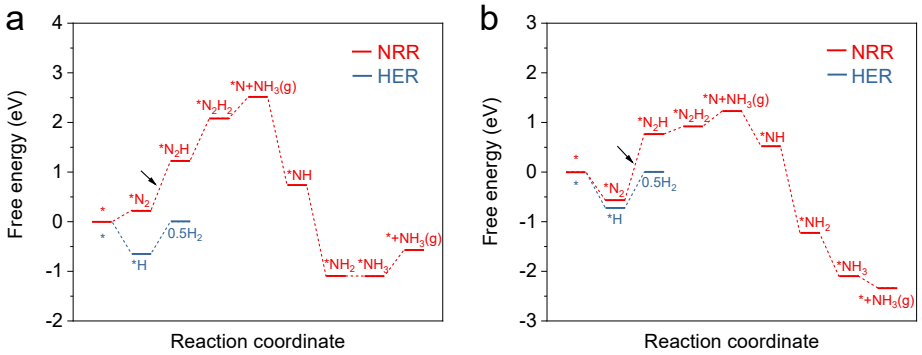

Fig. S18 Calculated free-energy diagrams of NRR and HER on (a) Au_S-TiO_2 and (b) Au_L-TiO_2.